Geophysical Research Letters

RESEARCH LETTER
10.1029/2019GL085951

Stochastic Parameterizations and the Climate Response to External Forcing: An Experiment With EC-Earth

Virna L. Meccia[1], Federico Fabiano[1], Paolo Davini[2], and Susanna Corti[1]

[1]Institute of Atmospheric Sciences and Climate (ISAC-CNR), Bologna, Italy, [2]Institute of Atmospheric Sciences and Climate (ISAC-CNR), Turin, Italy

Key Points:
- Abrupt collapse of winter sea ice in the Arctic is simulated by EC-Earth under RCP8.5 future scenario
- EC-Earth transient climate sensitivity is different when stochastic parameterizations are activated
- Transient climate sensitivity in stochastic runs changes radically as a function of the global mean temperature

Supporting Information:
- Supporting Information S1

Correspondence to:
V. L. Meccia,
V.Meccia@isac.cnr.it

Citation:
Meccia, V. L., Fabiano, F., Davini, P., & Corti, S. (2020). Stochastic parameterizations and the climate response to external forcing: An experiment with EC-Earth. *Geophysical Research Letters*, *47*, e2019GL085951. https://doi.org/10.1029/2019GL085951

Received 22 OCT 2019
Accepted 15 JAN 2020
Accepted article online 21 JAN 2020

Abstract The impacts of including stochastic physics schemes (SPS) in the atmospheric component of the EC-Earth climate model is studied by analyzing coupled simulations from 1850 to 2160. Sea ice in the Arctic retreats more slowly when SPS are included. An abrupt loss of winter sea ice is simulated 10 years later if the SPS are activated. However, this abrupt collapse is associated with a global surface air temperature (GSAT) of 17.4 ± 0.35 °C in all the cases. While the transient climate sensitivity is smaller if SPS are included up to the end of the 21st century, the opposite occurs in a warmer climate and in the absence of Arctic sea ice all the year-round. These results are explained by the skewed interaction between stochastic perturbations and the process of condensation. Under a warmer climate, tropical convection is enhanced with SPS leading to the formation of high-level clouds, which further increases GSAT.

Plain Language Summary Global climate models are a powerful tool to study the current climate and its future projections. Applying those models in high resolution is computationally demanding. A cheaper alternative to grid refinement is the use of stochastic physics schemes in which the unresolved subgrid processes are parameterized by introducing a term of randomness into the physical parameterizations. In this work, we study the impacts of including stochastic physics schemes in the atmospheric component of the EC-Earth climate model by analyzing long-term coupled simulations from 1850 to 2160. It was found that the global temperature increase is lower when the stochastic physics is included, which implies reduced climate sensitivity. However, with the melting of Arctic sea ice, the opposite occurs. An increase of high-clouds due to the skewed interaction between stochastic perturbations and the process of condensation accelerates the increase in temperature in the simulations with stochastic physics.

1. Introduction

The Arctic sea ice is a sensitive indicator of changes in global climate. Global climate models predict an overall decline of the Arctic sea ice extent, estimating that the Arctic will likely become seasonally ice-free in few decades (Jahn et al., 2016; Massonnet et al., 2012; Notz & Stroeve, 2016; Overland & Wang, 2013; Stroeve et al., 2007; Stroeve & Notz, 2018; Wang & Overland, 2009, 2012). However, there is still a large spread among model estimates of the state of the sea ice cover in the Arctic for the 21st century. Indeed, September sea ice is predicted to disappear between 2040 and 2060 under RCP8.5 scenario (Hezel et al., 2014; Huang et al., 2017; Massonnet et al., 2012; Wang & Overland, 2012), while a sea-ice-free Arctic in March may be found between 2134 and 2234 (Hezel et al., 2014). Moreover, the Arctic sea ice cover can experience an abrupt collapse in winter, which may be explained by a threshold-driven mechanism in which radiative feedbacks are not necessary (Drijfhout et al., 2015). While the Earth gets warmer, the sea ice becomes thinner. The areas with a very thin ice thickness can quickly collapse if warming continues and temperatures in winter do not reach the freezing point. The abrupt collapse of the sea ice cover is a winter feature and it does not occur in summer.

Recent studies suggest that increasing resolution in climate models may be necessary to correctly resolve key processes in the Arctic Ocean interface (e.g., Docquier et al., 2019). A computationally cheaper alternative to increasing resolution is represented by the application of stochastic physics schemes (SPS) in which the treatment of tendencies due to unresolved processes is parameterized by stochastic terms (Lorenz, 1975; Palmer, 2001; Pitcher, 1977). By introducing a term of randomness into the equations, SPS aim at representing the variability of the unresolved subgrid scale processes.

Currently, operational weather and climate centers use SPS routinely to make ensemble predictions from medium-range to seasonal time scales (e.g., Berner et al., 2009; Bowler et al., 2009; Charron et al., 2010; Weisheimer et al., 2014). SPS have been shown a potential capability of improving the mean state of the simulated climate (Berner et al., 2012; Palmer, 2012) by reducing model bias (Berner et al., 2017). Improvements were also found in simulating both tropical (Lin & Neelin, 2000, 2003; Watson et al., 2017) and extratropical (Dawson & Palmer, 2015) climate variability. Potential effects of SPS in coupled climate models are less investigated. It has been shown that they can correct long-standing mean-state biases (Sanchez et al., 2016) and improve the representation of El Niño–Southern Oscillation internal variability in the Community Earth System Model (Christensen et al., 2017) and the EC-Earth climate model (Yang et al., 2019). Moreover, the climate sensitivity might be affected by the inclusion of small-scale fluctuations in coupled simulations (Seiffert & von Storch, 2008). Recently, Strommen et al. (2019) demonstrated that the inclusion of SPS in the atmospheric component of EC-Earth coupled runs, reduces by 10% the global warming in the period 1850–2100 under the RCP8.5 future scenario. This result is associated with a smaller rate of decrease in the area covered by low-level clouds, which are known for having a negative radiative forcing (i.e., they have a net cooling effect; section 7.2.1.2 in Boucher et al., 2013). Strommen et al. (2019) argue that by turning on the SPS in EC-Earth, the cloud liquid water increases due to the "skewed" interaction between the stochastic perturbations and the process of condensation. A perturbation of temperature or humidity in one direction might produce condensation of a parcel of air, which is close to saturation. Conversely, a perturbation in the opposite direction would not change the cloud liquid water. This asymmetry translates into a different transient climate sensitivity in the same climate model depending on whether the SPS are activated or not.

In this study, we analyze the effects of including SPS in the atmospheric component of the EC-Earth model on the evolution of the sea ice extent in the Arctic during long-term coupled simulations covering the historical and future periods. In light of the results obtained, we further explore the dependence of the transient climate sensitivity on the global mean surface temperature (GSAT) and how it can be modified by the inclusion of SPS. In section 2, a description of the simulations used in this study is presented, while the results regarding the evolution of the sea ice cover in the Arctic and the changes in the transient climate sensitivity are presented in section 3. Concluding remarks are discussed in section 4.

2. Simulations

The experiments analyzed in this study are part of the Climate Stochastic Physics High-resolutioN eXperiments (Climate SPHINX) project which aimed at evaluating the impact of model resolution and stochastic parameterizations on the simulated climate (for details, see Davini et al., 2017). Simulations were carried out using version 3.1 of the EC-Earth climate model (Hazeleger et al., 2010, 2012). The atmospheric component consists of the cycle 36r4 Integrated Forecast System (ECMWF, 2009) model whereas the ocean one consists of the Nucleus for European Modelling of the Ocean (NEMO 3.3.1; Madec, 2008) model, which includes the Louvain la Neuve (LIM3; Vancoppenolle et al., 2012) sea ice model. LIM3 is a five-category sea ice thickness, enthalpy, salinity, and age distribution model. The vertical ice growth and decay in each thickness category are determined by an energy-conserving thermodynamic model with one layer of snow and five layers of ice (Vancoppenolle et al., 2009). The coupling between the atmospheric and oceanic components is done through OASIS3 (Valcke, 2013), with a coupling frequency of 3 hr. The Integrated Forecast System spatial resolution is T255 L91, which corresponds to a horizontal resolution of about 80 km at the equator and 91 vertical levels represented in a hybrid coordinate system. The model configuration in NEMO is the ORCA1L46, a tripolar grid with an average horizontal resolution of 1° × 1° and 46 vertical levels.

Six coupled climate simulations have been performed: three ensemble members constitute the control runs (*base*), while three ensemble members include SPS (*stoc*). For the latter, both the Stochastically Perturbed Parameterization Tendencies (SPPT) scheme (Buizza et al., 1999) and the Stochastic Kinetic Energy Backscatter (SKEB) scheme (Palmer et al., 2009) are incorporated in the atmospheric component of EC-Earth. The SPPT scheme acts on the tendencies of the physical fields by the application of multiplicative noise to the tendencies resulting from parameterized processes. The perturbation field is generated using a spectral pattern generator (Berner et al., 2009) that varies in space smoothly. SPPT is applied to the

tendencies of temperature, winds, and specific humidity and it aims at representing the model uncertainty associated with the parameterization schemes of radiation, turbulence, and gravity wave drag, nonorographic gravity wave drag, convection and large-scale water processes. The SKEB scheme was developed to represent the upscale transfer of energy that is observed in the real atmosphere but is underrepresented in forecast models, (Berner et al., 2009; Shutts, 2005). It estimates the kinetic energy lost in the model due to dissipation at the smallest scales and scatters this energy upscale by perturbing the streamfunction at the largest scales. SKEB scheme also uses a spectral pattern generator to create a perturbation field that is spatially and temporally correlated. The generated field is added at each time step to the deterministic stream function tendency.

SPHINX simulations span from 1850 to 2100. The strategy to construct the initial conditions is described in Davini et al. (2017). Historical forcing (1850–2005) is consistent with the Coupled Model Intercomparison Project, phase 5 (CMIP5) protocol (Taylor et al., 2012) and the future scenario (2006–2100) corresponds to the CMIP5 RCP8.5. For this paper, we extended each run for 60 years using the same model code and configuration as in Davini et al. (2017). The RCP8.5 setup has been followed for the greenhouse gas emissions, while the ozone values of the year 2100 were kept constant during the extended period. In this way, six 310-year (1850–2160) simulations have been obtained.

3. Results

3.1. Arctic Sea Ice

The seasonal cycle of sea ice extent lags the insolation cycle by ~3 months so that September (March) is the month of minimum (maximum) Arctic sea ice cover. Time series from 1850 to 2160 of sea ice extent in the Northern Hemisphere (NH) for September and March are plotted in Figures 1a and 1b, respectively. The sea ice extent is defined as the area of ocean where at least 15% of the surface is frozen: the grid area with sea ice cover higher than 0.15 are summed up. The three curves in blue (red) correspond to each ensemble member of the *base* (*stoc*) experiments. The overall trend of Arctic sea ice extent in September is negative (Figure 1a). Values from around 10×10^6 km^2 at the beginning of the simulations to 8×10^6 km^2 at the end of the historical period (2005) are simulated by all the six ensemble members. The reduction of the sea ice cover is stronger for the future than for the historical period and the two sets of runs begin to behave differently from 2030 onward: The *base* experiments show a faster decrease than the *stoc* ones. As a consequence, an ice-free Arctic (less than 1×10^6 km^2 of sea ice extent for at least 5 consecutive years) in September is reached in 2075 ± 2 for the *base* experiments and about a decade later (in 2083 ± 3) for the *stoc* experiments (Figure 1a).

The sea ice extent in March (Figure 1b) also shows a general decline, the trend being stronger during the future scenario than during the historical period. Values are roughly between 15 and 16×10^6 km^2 at the beginning of the simulations, and they are characterized by a weak negative trend until 1975, approximately. Afterward, the decrease intensifies reaching a sea ice extent of about 12×10^6 km^2 in 2060. After 2060, the two sets of experiments diverge rapidly: Reduction of sea ice extent occurs faster (rate of 0.14 vs. 0.09 km^2/yr from 2060 to 2095) in the *base* experiments than in the *stoc* ones. Moreover, all the ensemble members simulate an abrupt sea ice loss in March (Figure 1b) that occurs about 10 years later in the *stoc* runs (2106 ± 2) than in the *base* ones (2096 ± 2). Once the abrupt collapse has taken place in all the cases, the trajectories of the two families of experiments converge and behave similarly from then on. The Arctic free of sea ice in March is obtained around 2151 ± 3 (2153 ± 1) in the *base* (*stoc*) runs.

According to Drijfhout et al. (2015), the abrupt collapse of winter sea ice in the Arctic occurs after crossing a threshold value of GSAT (represented by an increment of global temperature from the preindustrial period ranging between 4.5 and 8.2 °C) which, for the CMIP5 simulations, is only reached under RCP8.5 future scenario. To find the threshold value in EC-Earth, we constructed the state space diagrams of the sea ice area in the Arctic versus GSAT (Figure 2). Each panel corresponds to one ensemble member; upper (lower) panels show the results for the *base* (*stoc*) experiments. For this analysis, we consider the seasonal average sea ice area north of 75°N. Changes in the sea ice area are fastest during the months March-April-May (MAM) because its seasonal cycle responds to the solar radiation with a time lag of ~3 months. At first glance, it emerges that even though the occurrence of the abrupt collapse in *stoc* and *base* is lagged by about 10 years (Figure 1b), the two configurations have a similar threshold temperature. Indeed, the decline of the winter sea ice seems to occur in three phases for all the six runs: two gradual decreases—associated with relatively

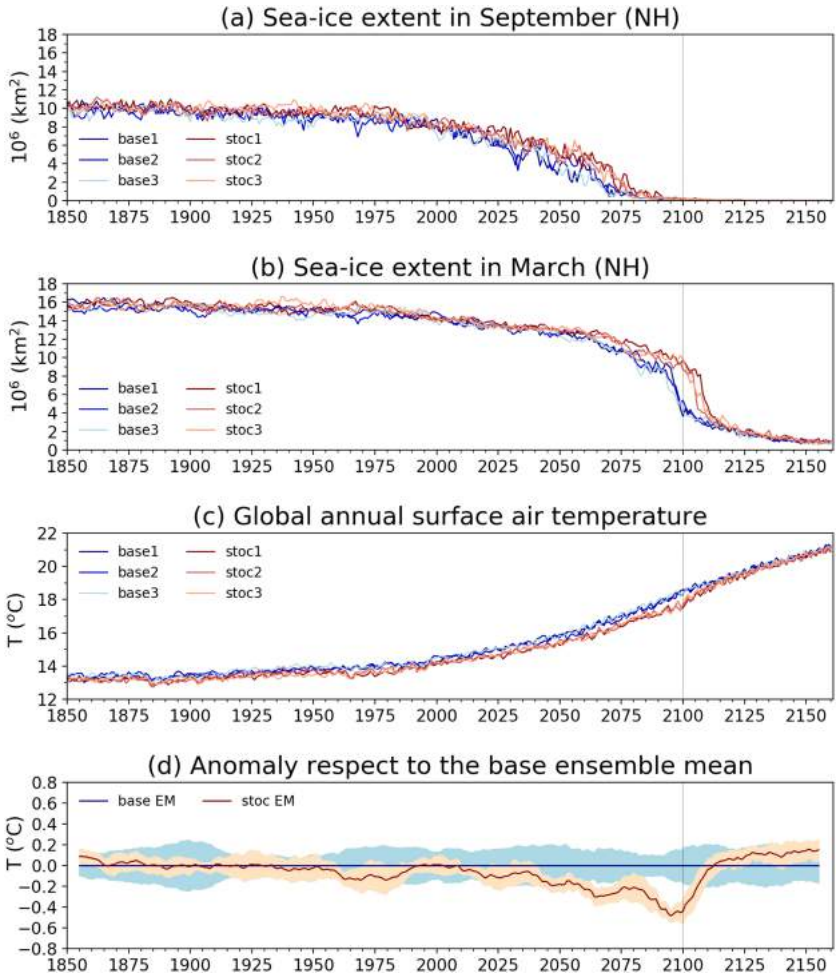

Figure 1. Results of the simulations from 1850 to 2160. NH sea ice extent in (a) September and (b) March; (c) GSAT (°C) and (d) difference with respect to the base ensemble mean of the GSAT increment (°C). Ten-year moving averaged ensemble means and the ensemble members' spreads are plotted in (d). All three ensemble members for the *base* (*stoc*) experiments are plotted in blue (red). The gray vertical line indicates when the original runs end and the extended simulation starts.

low and high temperatures—and an abrupt change occurring around the threshold temperature. To identify the value of temperature in which the slope changes, the *z* shape curve was fit with three straight lines minimizing the root square error. The first change in the slope is associated with temperatures in which the abrupt sea ice collapse occurs, and it is marked as a vertical gray line in each panel of Figure 2. The GSAT that can be considered as the threshold value for the abrupt decline of winter sea ice cover is 17.4 °C, with a standard deviation among the ensemble members of 0.35 °C. This value corresponds to an increment in global temperature from the preindustrial period of about 4 °C, which is slightly smaller than the values found by Drijfhout et al. (2015).

3.2. Global Temperature

Because the boundary conditions are the same for all the simulations, previous findings regarding the timing of the sea ice decrease/collapse in the Arctic imply that the model climate sensitivity is higher when the SPS are not included, as stated by Strommen et al. (2019). The time series of GSAT for the six ensemble members (*base* in blue; *stoc* in red) is plotted in Figure 1c. To better distinguish the differences between both sets of experiments, the difference with respect to the *base* ensemble mean of the surface temperature increment (respect to the initial value) are plotted in Figure 1d: Here the blue line represents the difference of the *base* ensemble mean respect to itself (always zero). The red line represents the difference of the *stoc* ensemble

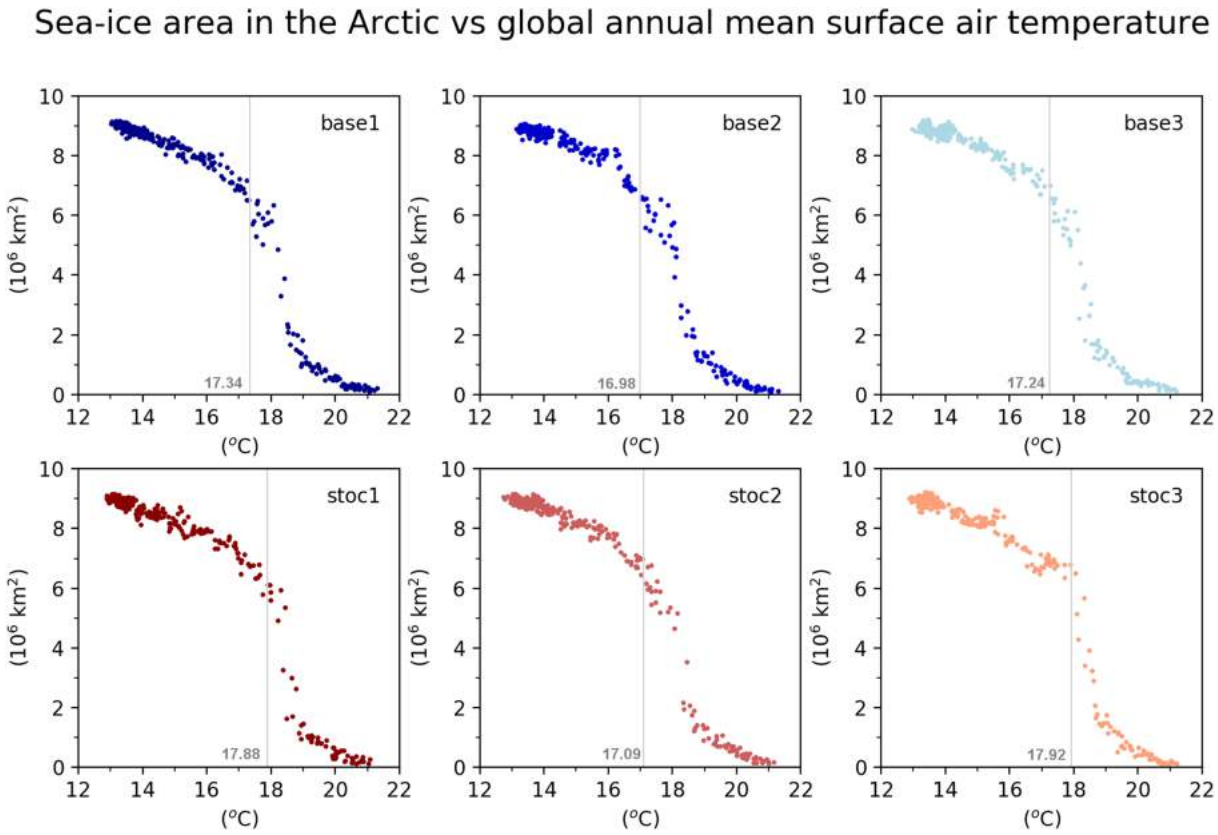

Figure 2. Sea ice area in the Arctic versus GSAT for each experiment. Each dot represents a seasonal average over March-April-May (MAM) of 1 year. The threshold temperature value for the abrupt decline of winter sea ice is highlighted in gray.

mean respect to the *base* ensemble mean. The colored areas represent the ensemble members' spread. A 10-yr moving average is applied to each series. *Base* and *stoc* GSAT curves display a similar behavior during the first part of the historical period but they begin to drift apart by the second half of the 20th century (Figures 1c and 1d). The difference between the two sets of experiments reaches the maximum value around 2100 when the GSAT change (with respect to the initial value) is of about 0.5 °C larger in the *base* experiments than in the *stoc* ones (Figures 1c and 1d). Quite unexpectedly, after the year 2100, the opposite occurs: Global temperature increases faster in the *stoc* runs. By the end of 2155, the temperature increment with respect to the initial value is about 0.2 °C higher in the *stoc* runs than in the *base* ones (Figure 1d).

It is apparent that the transient climate sensitivity is lower when the SPS are activated only during the 21st century. Curiously, the situation reverses at the beginning of the 22nd century, coinciding with the simulated free sea ice conditions in the Arctic throughout the year. Strommen et al. (2019) have associated the smaller transient climate sensitivity of the *stoc* runs with changes in the low-level cloud cover (LCC) feedback. LCC versus the GSAT is plotted in Figure 3a. Blue dots are associated with the *base* ensemble mean whereas the *stoc* ensemble mean is shown as red dots. In both experiments, LCC decreases when GSAT increases up to a value of about 18.5 °C (Figure 3a), which occurs shortly after the year 2100 (Figure 1c). However, the decline of this variable with global warming is steeper for the *base* than for the *stoc* runs (Figure 3a). The LCC response to global warming represents a positive feedback for the system (Bony et al., 2015), which is larger in the *base* runs until 2100, yielding a larger temperature increase. For temperatures higher than 18.5 °C, the trend of LCC with GSAT becomes much smaller and the correlation between LCC and temperature decreases.

In summary, before 2100 the transient temperature increment is larger in the *base* runs than in the *stoc* ones and this seems to be due to a different amplitude of the LCC feedback (positive and larger in the *base* runs),

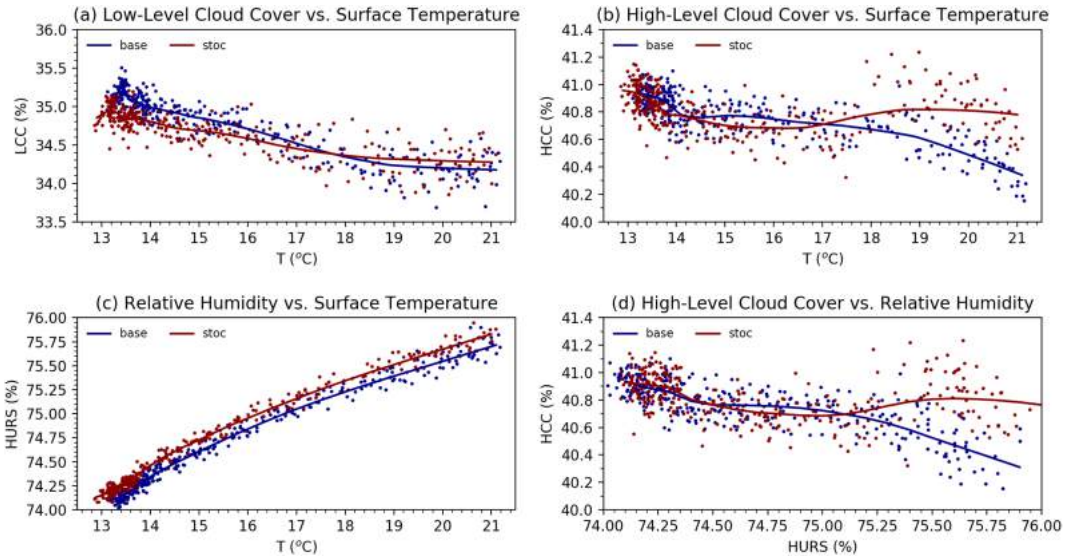

Figure 3. Globally averaged (a) LCC; (b) HCC and (c) surface relative humidity (HURS) versus the GSAT; and (d) HCC versus HURS for the ensemble mean of the *base* (blue) and *stoc* (red) experiments. Solid lines are the results of a nonparametric regression method (locally estimated scatterplot smoothing).

as assessed by Strommen et al. (2019). However, a different picture arises after 2100: The rate of increase in temperature in the *stoc* simulations steepens and the red curve in Figure 1d catches up with the blue one and even exceeds it. This fact is also reflected in the energy budget (Figure S1 in the supporting information), which shows a higher net surface (incoming) radiation in the *stoc* respect to the *base* runs. Therefore, the LCC argument does not apply anymore. Indeed, the LCC (positive) feedback is much weaker after the year 2100 for the two sets of experiments and does not explain the differences in the two responses (Figure 3a).

The larger energy imbalance of the *stoc* runs is explained by lower upward thermal radiation at the top of the atmosphere. This can be associated with an increase in the area covered by high-level clouds (HCC), which reflect little sunlight but since they have a low emission temperature, they warm the surface more than they cool it (section 7.2.1.2 in Boucher et al., 2013). The relation between HCC and GSAT is shown in Figure 3b. For GSAT lower than ~17 °C, higher values of HCC are found in the *base* runs. However, when GSAT crosses this threshold value, HCC level in the *stoc* experiments equals that in the *base* ones, and the derivative of the red curve in Figure 3b become positive. This leads to an enhanced production of HCC with temperatures higher than 17 °C, which in turn contributes to a further increase of warming (positive feedback). This positive feedback in the *stoc* runs triggers the sudden temperature increment (Figure 1d).

The increase in the production of HCC in the *stoc* simulations mainly occurs at low-latitudes (Figure S2), and it is associated with a decrease in the outgoing longwave radiation. This is consistent with intensified deep convection along the tropical oceans. In fact, the *stoc* runs show a sharp transition in the amount of HCC at tropical latitudes (Figure S2) in the years around 2100, suggesting a regime change in the rate of tropical deep convection. The interaction between the random perturbations in temperature or humidity (introduced by the inclusion of SPS) with the process of condensation of an air parcel close to saturation can explain this outcome. For instance, we found that the global surface relative humidity increases with warming (Figure 3c), going from 74% up to 76%. This increment is simulated in all the runs, it is roughly linear for temperatures higher than ~17 °C, and it is similar for both sets of experiments, *base* and *stoc*. So, it is possible that once a certain critical threshold of relative humidity is achieved, SPS foster the development of convective events. In other words, given a parcel of air close to saturation (with a relatively high value of relative humidity), the stochastic perturbations might favor condensation by perturbing the system in that direction. Indeed, there is a strong relationship between the HCC and the surface relative humidity (Figure 3d), which is particularly strong in the tropics (Figures S3 and S4) where deep convective events take place. Such a tipping point occurs at about 75% of relative humidity and will be investigated in a forthcoming study.

4. Final Remarks

We investigated the impacts of including stochastic physics schemes (SPPT/SKEB) in the atmospheric model component of the EC-Earth climate model on the simulated sea ice retreat in the Arctic. A set of three-member ensemble experiments (*base* and *stoc*) has been analyzed. The period of simulation spans from 1850 to 2160 and the RCP8.5 scenario is used for the future forcing. We found that the response of the Arctic sea ice retreat to the same imposed radiative forcing is different in the two sets of experiments: the Arctic sea ice rate of decline is higher in the *base* experiments than in the *stoc* ones. In our simulations, the Arctic appears free of sea ice in September around 2075 $\pm$ 2 or even later, in 2083 $\pm$ 3, if the SPS are activated. These values are slightly higher than the ones reported in the literature. Nonetheless, Massonnet et al. (2012) concluded that the year at which the September sea ice extent drops below a certain value correlates well with the initial sea ice properties. Our initial state of September sea ice extent in 1850 (~10×10^6 km^2 in both, *base* and *stoc*) is higher than the CMIP5 models ensemble mean (~8×10^6 km^2; Hezel et al., 2014). This fact might delay the melting in the EC-Earth simulations respect to the CMIP5 ensemble mean. On the other hand, we have obtained that the Arctic appears free of sea ice all the year-round after 2153. This value is inside the range reported in the literature for the annually ice-free conditions (Hezel et al., 2014).

The winter sea ice extent experiences an abrupt collapse in all the ensemble members, and it is related to a value of GSAT of 17.4 $\pm$ 0.35 °C. This value is in the lower limit of the range previously found, roughly [17.5 °C; 21.5 °C], using nine CMIP5 models (Figure 2 of Bathiany et al., 2016). Somehow, unexpectedly, it was found that such value also represents a sort of tipping point for the model transient climate sensitivity: below this temperature, the global warming of the *stoc* runs is lower than the *base* ones (as shown by Strommen et al., 2019), while above this threshold the opposite becomes true. This behavior can be explained by the skewed interaction between the stochastic perturbations and the process of condensation. The low-level clouds production is affected during the first three-quarters of the simulations (until the year 2100 circa). However, in a warmer climate (GSAT higher than ~17 °C), the surface relative humidity in the tropics is particularly high. As a result, the stochastic perturbations in those regions highly affect deep convection producing a larger amount of high-level clouds that contribute to positive feedback. The sensitivity of deep convection to SPS increases with time in a warming climate.

It is worth noting that the regime shift occurs at about the same value of GSAT that represents the threshold value for the abrupt collapse of winter sea ice in the Arctic. Although the timing of these two dramatic shifts (i.e., the abrupt decline of winter sea ice and the swift high-level clouds formation) is remarkable, there is no evident physical mechanism that could tie the two processes. The two abrupt changes might be independent responses to a given level of global warming. In conclusion, including SPS in EC-Earth yields differences not only in the simulated mean climate but also in the path that the model travels along its phase space to achieve it.

Finally, we want to highlight that even though SPS attempt to represent the subgrid processes, there is still large uncertainty in the climate response to external forcing that cannot be reduced, neither by the inclusion of SPS nor by increasing resolution. In this sense, we think that more efforts need to be made to understand the link between subgrid processes and its response to external forcing.

Acknowledgments
The authors acknowledge support by the PRIMAVERA and TiPES projects of the Horizon 2020 Research Programme, funded by the European Commission under Grant Agreements 641727 and 820970, respectively. The SPHINX data were generated with computing resources provided by CINECA and LRZ in the framework of Climate SPHINX and Climate SPHINX reloaded PRACE projects. The extension of the SPHINX scenarios have been carried out at ECMWF under the special project SPITMECC. Details on the data accessibility are available on the Climate SPHINX project official website (http://www.to.isac.cnr.it/sphinx/).

References

Bathiany, S., Notz, D., Mauritsen, T., Raedel, G., & Brovkin, V. (2016). On the potential for abrupt Arctic winter sea ice loss. *Journal of Climate*, *29*(7), 2703–2719. https://doi.org/10.1175/JCLI-D-15-0466.1

Berner, J., Achatz, U., Batte, L., Bengtsson, L., de la Cámara, A., Christensen, H., et al. (2017). Stochastic parameterization: Towards a new view of weather and climate models. *Bulletin of the American Meteorological Society*, *98*(3), 565–588. https://doi.org/10.1175/BAMS-D-15-00268.1

Berner, J., Jung, T., & Palmer, T. (2012). Systematic model error: The impact of increased horizontal resolution versus improved stochastic and deterministic parameterizations. *Journal of Climate*, *25*, 4946–4962. https://doi.org/10.1175/JCLI-D-11-00297.1

Berner, J., Shutts, G., Leutbecher, M., & Palmer, T. (2009). A spectral stochastic kinetic energy backscatter scheme and its impact on flow-dependent predictability in the ECMWF ensemble prediction system. *Journal of the Atmospheric Sciences*, *66*, 603–626. https://doi.org/10.1175/2008JAS2677.1

Bony, S., Stevens, B., Frierson, D. M., Jakob, C., Kageyama, M., Pincus, R., et al. (2015). Clouds, circulation and climate sensitivity. *Nature Geoscience*, *8*(4), 261–268. https://doi.org/10.1038/ngeo2398

Boucher, O., Randall, D., Artaxo, P., Bretherton, C., Feingold, G., Forster, P., Kerminen, V.-M., Kondo, Y., Lia, H, Lohmann, o, U., Rasch, P. , Satheesh, S.K., Sherwood, S., Stevens, B., Zhang, X.Y. (2013). In Climate Change 2013: The Physical Science Basis. In T. F. Stocker, D. Qin, G.-K. Plattner, M. Tignor, S. K. Allen, J. Doschung, A. Nauels, Y. Xia, V. Bex, & P. M. Midgley (Eds.), *Contribution of Working Group*

I to the Fifth Assessment Report of the Intergovernmental Panel on Climate Change. United Kingdom andNew York, NY, USA: Cambridge University Press. pp. 571-657. https://doi.org/10.1017/CBO9781107415324.016

Bowler, N. E., Arribas, A., Beare, S. E., Mylne, K. R., & Shutts, G. J. (2009). The local ETKF and SKEB: upgrade to the MOGREPS short-range ensemble prediction system. *Quarterly Journal of the Royal Meteorological Society*, *135*, 767–776. https://doi.org/10.1002/qj.394

Buizza, R., Miller, M., & Palmer, T. N. (1999). Stochastic representation of model uncertainties in the ECMWF ensemble prediction system. *Quarterly Journal of the Royal Meteorological Society*, *125*, 2887–2908. https://doi.org/10.1002/qj.49712556006

Charron, M., Pellerin, G., Spacek, L., Houtekamer, P. L., Gagnon, N., Mitchell, H., & L, et al. (2010). Toward random sampling of model error in the Canadian ensemble prediction system. *Monthly Weather Review*, *138*, 1877–1901. https://doi.org/10.1175/2009MWR3187.1

Christensen, H. M., Berner, J., Coleman, D., & Palmer, T. N. (2017). Stochastic parameterization and the El Niño–Southern Oscillation. *Journal of Climate*, *30*, 17–38. https://doi.org/10.1175/JCLI-D-16-0122.1

Davini, P., von Hardenberg, J., Corti, S., Christensen, H. M., Juricke, S., Subramanian, A., et al. (2017). Climate SPHINX: evaluating the impact of resolution and stochastic physics parameterisations in the EC-Earth global climate model. *Geoscientific Model Development*, *10*(3), 1383–1402. https://doi.org/10.5194/gmd-10-1383-2017

Dawson, A., & Palmer, T. N. (2015). Simulating weather regimes: impact of model resolution and stochastic parametrisation. *Climate Dynamics*, *44*(7-8), 2177–2193. https://doi.org/10.1007/s00382-014-2238-x

Docquier, D., Grist, J. P., Roberts, M. J., Roberts, C. D., Semmler, T., Posoni, L., et al. (2019). Impact of model resolution on Arctic sea ice and North Atlantic Ocean heat transport. *Climate Dynamics*, *53*(7–8), 4989–5017. https://doi.org/10.1007/s00382-019-04840-y

Drijfhout, S., Bathiany, S., Beaulieu, C., Brovkin, V., Claussen, M., Huntingford, C., et al. (2015). Catalogue of abrupt shifts in Intergovernmental Panel on Climate Change climate models. *Proceedings of the National Academic of Sciences of the United States of America*, *112*(43), E5777–E5786. https://doi.org/10.1073/pnas.1511451112

ECMWF (2009), IFS cycle36r1, https://www.ecmwf.int/en/forecasts/documentation-and-support/changes-ecmwf-model/ifs-documentation, European Center for Medium Range Forecast.

Hazeleger, W., Severijns, C., Semmler, T., Ştefăănescu, S., Yang, S., Wang, X., et al. (2010). EC-Earth: A seamless Earth-system prediction approach in action. *Bulletin of the American Meteorological Society*, *91*(10), 1357–1364. https://doi.org/10.1175/2010BAMS2877.1

Hazeleger, W., Wang, X., Severijns, C., Ştefănescu, S., Bintanja, R., Sterl, A., et al. (2012). EC-Earth V2.2: description and validation of a new seamless Earth system prediction model. *Climate Dynamics*, *39*(11), 2611–2629. https://doi.org/10.1007/s00382-011-1228-5

Hezel, P. J., Fichefet, T., & Massonnet, F. (2014). Modeled Arctic sea ice evolution through 2300 in CMIP5 extended RCPs. *The Cryosphere*, *8*, 1195–1204. https://doi.org/10.5194/tc-8-1195-2014

Huang, F., Zhou, X., & Wang, H. (2017). Arctic sea ice in CMIP5 climate model projections and their seasonal variability. *Acta Oceanologica Sinica*, *36*(8), 1–8. https://doi.org/10.1007/s13131-017-1029-8

Jahn, A., Kay, J. E., Holland, M. M., & Hall, D. M. (2016). How predictable is the timing of a summer ice-free Arctic? *Geophysical Research Letters*, *43*, 9113–9120. https://doi.org/10.1002/2016GL070067

Lin, J. W.-B., & Neelin, J. D. (2000). Influence of a stochastic moist convective parameterization on tropical climate variability. *Geophysical Research Letters*, *27*, 3691–3694. https://doi.org/10.1029/2000GL011964

Lin, J. W.-B., & Neelin, J. D. (2003). Toward stochastic deep convective parameterization in general circulation models. *Geophysical Research Letters*, *30*, 1162. https://doi.org/10.1029/2002GL016203

Lorenz, E. N. (1975). *Climatic predictability. In The physical basis of climate and climate modelling*. Geneva: WMO GARP Publication Series No 16, World Meteorological Organisation.

Madec, G. (2008). NEMO ocean engine. Technical report, Institut Pierre-Simon Laplace (IPSL).

Massonnet, F., Fichefet, T., Goosse, H., Bitz, C. M., Philippon-Berthier, G., Holland, M. M., & Barriat, P.-Y. (2012). Constraining projections of summer Arctic sea ice. *The Cryosphere*, *6*(6), 1383–1394. https://doi.org/10.5194/tc-6-1383-2012

Notz, D., & Stroeve, J. (2016). Arctic sea ice loss directly follows cumulative anthropogenic CO_2 emissions. *Science*, *354*(6313), 747–750. https://doi.org/10.1126/science.aag2345

Overland, J. E., & Wang, M. (2013). When will the summer Arctic be nearly sea ice free? *Geophysical Research Letters*, *40*(10), 2097–2101. https://doi.org/0.1002/grl.50316

Palmer, T.N. (2001). A nonlinear dynamical perspective on model error: A proposal for non-local stochastic-dynamic parametrization in weather and climate prediction models. *Quarterly Journal of the Royal Meteorological Society, 127 (*572*),* 279–304. https://doi.org/10.1002/qj.49712757202

Palmer, T. N. (2012). Towards the probabilistic Earth-system simulator: A vision for the future of climate and weather prediction. *Quarterly Journal of the Royal Meteorological Society*, *138*(665), 841–861. https://doi.org/10.1002/qj.1923

Palmer, T.N., Buizza, R. Doblas-Reyes, F. Jung, T. Leutbecher, M., Shutts, G.J., et al.. (2009). Stochastic parametrization and model uncertainty. ECMWF Technical Report 598, 44 pp. [Available online at https://www.ecmwf.int/en/elibrary/11577-stochastic-parametrization-and-model-uncertainty].

Pitcher, E. J. (1977). Application of stochastic dynamic prediction to real data. *Journal of the Atmospheric Sciences*, *34*(1), 3–21. https://doi.org/10.1175/1520-0469(1977)034<0003:AOSDPT>2.0.CO;2

Sanchez, C., Williams, K. D., & Collins, M. (2016). Improved stochastic physics schemes for global weather and climate models. *Quarterly Journal of the Royal Meteorological Society*, *142*, 147–159. https://doi.org/10.1002/qj.2640

Seiffert, R., & von Storch, J.-S. (2008). Impact of atmospheric small-scale fluctuations on climate sensitivity. *Geophysical Research Letters*, *35*, L01609. https://doi.org/10.1029/2008GL033483

Shutts, G. J. (2005). A kinetic energy backscatter algorithm for use in ensemble prediction systems. *Quarterly Journal of the Royal Meteorological Society*, *131*, 3079–3102. https://doi.org/10.1256/qj.04.106

Stroeve, J., Holland, M. M., Meier, W., Scambos, T., & Serreze, M. (2007). Arctic sea ice decline: faster than forcast. *Geophysical Research Letters*, *34*, L09501. https://doi.org/10.1029/2007GL029703

Stroeve, J. C., & Notz, D. (2018). Changing state of Arctic sea ice across all seasons. *Environmental Research Letters*, *13*(10), 103001. https://doi.org/10.1088/1748-9326/aade56

Strommen, K., Watson, P. A. G., & Palmer, T. N. (2019). The impact of a stochastic parameterization scheme on climate sensitivity in EC-Earth. *Journal of Geophysical Reearch-Atmosphere*, *124*. https://doi.org/10.1029/2019JD030732

Taylor, K., Stouffer, R., & Meehl, G. (2012). An overview of CMIP5 and the experiment design. *Bulletin of the American Meteorological Society*, *93*, 485–498. https://doi.org/10.1175/BAMS-D-11-00094.1

Valcke, S. (2013). The OASIS3 coupler: A European climate modelling community software. *Geoscientific Model Development*, *6*, 373–388. https://doi.org/10.5194/gmd-6-373-2013

Vancoppenolle, M., Bouillon, S., Fichefet, T., Goosse, H., Lecomte, O., Morales Maqueda, M., Madec G. (2012). LIM, The Louvain-la-Neuve sea ice model, Notes du Pôle de modélisation.

Vancoppenolle, M., Fichefet, T., Goosse, H., Bouillon, S., Madec, G., & Morales Maqueda, M. A. (2009). Simulating the mass balance and salinity of Arctic and Antarctic sea ice. 1. Model description and validation. *Ocean Modelling*, *27*, 33–53. https://doi.org/10.1016/j.ocemod.2008.10.00

Wang, M., & Overland, J. E. (2009). A sea ice free summer Arctic within 30 years? *Geophysical Research Letters*, *36*, L07502. https://doi.org/10.1029/2009GL037820

Wang, M., & Overland, J. E. (2012). A sea ice free summer Arctic within 30 years: An update from CMIP5 models. *Geophysical Research Letters*, *39*(18), L18501. https://doi.org/10.1029/2012GL052868

Watson, P. A. G., Berner, J., Corti, S., Davini, P., von Hardenberg, J., Sanchez, C., et al. (2017). The impact of stochastic physics on tropical rainfall variability in global climate models on daily to weekly time scales. *Journal of Geophysical Research - Atmospheres*, *122*(11), 5738–5762. https://doi.org/10.1002/2016JD026386

Weisheimer, A., Corti, S., Palmer, T. N., & Vitart, F. (2014). Addressing model error through atmospheric stochastic physical parametrizations: Impact on the coupled ECMWF seasonal forecasting system. *Philosophical Transactions of The Royal Society A Mathematical Physical and Engineering Sciences*, *372A*, 20130290. https://doi.org/10.1098/rsta.2013.0290

Yang, C., Christensen, H. M., Corti, S., von Hardenberg, J., & Davini, P. (2019). The impact of stochastic physics on the El Niño Southern Oscillation in the EC-Earth coupled model. *Climate Dynamics*, *53*(5—6), 2843–2859. https://doi.org/10.1007/s00382-019-04660-0